Petroleum Science 21 (2024) 1969–1979

Contents lists available at ScienceDirect

Petroleum Science

journal homepage: www.keaipublishing.com/en/journals/petroleum-science

Original Paper

Temperature prediction model in multiphase flow considering phase transition in the drilling operations

Yang Zhang [a], Yong-An Li [a], Xiang-Wei Kong [b, **], Hao Liu [a], Teng-Fei Sun [a, *]

[a] College of Mechanical and Electrical Engineering, Beijing University of Chemical Technology, Beijing, 100027, China
[b] School of Petroleum Engineering, Yangtze University, Wuhan, 430000, Hubei, China

ARTICLE INFO

Article history:
Received 25 August 2023
Received in revised form
4 January 2024
Accepted 4 January 2024
Available online 6 January 2024

Edited by Jia-Jia Fei

Keywords:
Managed pressure drilling
Phase transition
Temperature
Gas-drilling mud two phase

ABSTRACT

The study considers gas compression properties, gas slippage, back pressure (BP), phase transition (PT), well depth, and differences in gas-liquid physical properties. A new temperature model for multiphase flow is proposed by considering phase transition in the drilling process. The mathematical model of multiphase flow is solved using the finite difference method with annulus mesh division for grid nodes, and a module for multiphase flow calculation and analysis is developed. Numerical results indicate that the temperature varies along the annulus with the variation of gas influx at the bottom of the well. During the process of controlled pressure drilling, as gas slips along the annulus to the wellhead, its volume continuously expands, leading to an increase in the gas content within the annulus, and consequently, an increase in the pressure drop caused by gas slippage. The temperature increases with the increase in BP and decreases in gas influx rate and wellbore diameter. During gas influx, the thermal conductivity coefficient for the gas-drilling mud two phases is significantly weakened, resulting in a considerable change in temperature along the annulus. In the context of MPD, the method of slightly changing the temperature along the annulus by controlling the back pressure is feasible.

1. Introduction

Pressure control drilling is accomplished by adjusting mud density, but the response of traditional pressure control methods is slow and imprecise (Lordejani et al., 2020). To overcome the shortcomings of conventional pressure control methods, Halliburton introduced Managed Pressure Drilling (MPD), and Weatherford introduced Drilling Fluid Micro-Flow Control (MFC) technology (Bu et al., 2011; Vieira et al., 2012). The primary objective of MPD is to offer a rapid, precise, and efficient method for bottom hole pressure control. On the other hand, MFC utilizes precise flow monitoring to detect overflow or wellbore leakage, followed by automatic choke adjustments to regulate the flow and meet the requirements of bottom hole pressure (Saeed et al., 2012; Bacon, 2011). Derived from MPD, MFC has its uniqueness, which enables it to detect early intrusion and loss, and predict and control related accidents more accurately. In comparison to MFC, MPD can detect a much smaller range of pressure fluctuations in the well (Choe and Juvkam-Wold, 1997).

During the drilling process, parameters such as wellbore temperature, drilling pressure, rheological properties, and cuttings concentration undergo changes (Yin et al., 2020). Hydraulic calculations and analysis are therefore crucial for the design of MPD. However, hydraulic calculations, including state equations, phase transition (PT), and gas migration along the annulus, are all temperature-dependent. Additionally, temperature influences changes in drilling fluid rheological properties, pump times, and mud density parameters (Hajidavalloo et al., 2021). This is particularly significant in high-temperature, high-pressure wells where density estimation differences can lead to inaccurate bottom hole pressure estimations, severely affecting downhole pressure control. In general, the negative impact of temperature on mud density outweighs the positive impact of pressure on mud density. Thus, research into the temperature field has consistently been a focal point of MPD studies (Tarvin et al., 1991; Kumar and Samuel, 2012; Pepin et al., 2004; Ataga and Ogbonna, 2012).

Fu et al. (2020) established a transient heat transfer and

* Corresponding author.
** Corresponding author.
E-mail addresses: 76922591@qq.com (X.-W. Kong), suntengfei@mail.buct.edu.cn (T.-F. Sun).

https://doi.org/10.1016/j.petsci.2024.01.004

multiphase flow mathematical model based on considering phase changes. Agwu proposed a method that utilizes an artificial neural network model to predict downhole density of oil-based mud under high-temperature and high-pressure conditions (Agwu et al., 2020). Wei et al. (2022) developed a multi-physics, non-equilibrium phase transition, and multiphase flow mathematical model considering temperature, pressure, and velocity. This model provides a better understanding of downhole fluid phase transition characteristics and the variations in multiphase flow behavior. Takalkar proposed the utilization of computational fluid dynamics tools to simulate complex two-dimensional and three-dimensional transient multiphase flow models. This approach enhances the computation of temperature, pressure, and velocity within the wellbore annulus and aids in advancing early kick detection (Sleiti et al., 2020).

Due to the increasing energy demand and the development of oil drilling technology, drilling of ultra-deep wells, high temperature and high pressure wells, and gas hydrate wells has become a crucial aspect of the drilling industry's development (Lin et al., 2013; Wu et al., 2011; Ramey Jr, 1962; Shiu and Beggs, 1980; Thompson and Burgess, 1985; Kabir and Hasan, 1991; Bennion and Bachu, 2006, 2008a). During the drilling process of deep and ultra-deep wells, the formation temperature increases with depthtypically at a geothermal gradient of 3′C per 100 m (Bennion and Bachu, 2008b; Yasunami, 2008).

According to the classification by the Society of Petroleum Engineers (SPE), the vast majority of deep and ultra-deep wells worldwide fall into the category of High Pressure High Temperature (HPHT) Class I and Ultra High Pressure High Temperature (UHPHT) Class II wells. Temperatures in these wells can reach up to 260 °C (Pu et al., 2022). As petroleum exploration advances into deeper and ultra-deep layers, conventional water-based drilling fluids and oil-based drilling fluids are no longer suitable for high-temperature and high-pressure geological formations (Li et al., 2022).

The increase in formation temperature results in elevated circulating drilling fluid temperature, which affects both the performance of drilling fluid and the service life of downhole tools, as well as the safety of drilling operations (Thiessen, 2017). The density, thermal conductivity, specific heat capacity, and viscosity of drilling fluids are all influenced by the wellbore temperature. Conversely, these same properties of drilling fluids also affect the distribution of wellbore temperature during the drilling process (Zhang et al., 2021). Therefore, it is crucial during the drilling process to promptly cool the drilling fluid in order to maintain the drilling fluid at an appropriate temperature.

The objective of this study is to investigate a new temperature model in multiphase flow by considering phase transition during drilling operations. This paper considers the gas compression properties, gas slippage, back pressure (BP), phase transition (PT), well depth, and gas-liquid physical property differences. It proposes a new temperature model in multiphase flow by considering phase transition during drilling operations. The mathematical model of multiphase flow is solved using the finite difference method with grid nodes obtained through annulus mesh division. Additionally, a calculation and analysis module for multiphase flow is developed.

2. The establishment of mathematical modeling

Due to the pressure difference, formation fluids of high temperature and pressure can invade the bottom of the well in reservoirs. Fig. 1 illustrates the process of controlled pressure drilling gas invading the bottom hole. The fluid in the figure consists of drilling fluid and gas phases.

2.1. The establishment of the pressure field model

Based on the characteristics of supercritical fluid, the model is developed with the following fundamental assumptions.

(i) According to decalescence and discharge heat of phase change, single dimension passes heat theory model of phase change is considered.
(ii) The temperature exhibits a symmetrical distribution around the wellbore and formation, with the temperature gradient in the formation being known.
(iii) The deformation of the drill string is disregarded during changes in pressure and temperature.

The annular pressure gradient equation is established based on the concept of multiphase flow in managed pressure drilling (MPD).

$$\frac{\mathrm{d}p}{\mathrm{d}H}=\left(\frac{\mathrm{d}p}{\mathrm{d}H}\right)_{\mathrm{gag}}+\left(\frac{\mathrm{d}p}{\mathrm{d}H}\right)_{\mathrm{flo}}+\left(\frac{\mathrm{d}p}{\mathrm{d}H}\right)_{\mathrm{arl}} \tag{1}$$

where, $\left(\frac{\mathrm{d}p}{\mathrm{d}H}\right)_{\mathrm{gag}}$ is weight component, $\left(\frac{\mathrm{d}p}{\mathrm{d}H}\right)_{\mathrm{flo}}$ is acceleration component, $\left(\frac{\mathrm{d}p}{\mathrm{d}H}\right)_{\mathrm{anl}}$ is friction forces component.

2.2. The establishment of the temperature field model

By selecting a micro element in the annulus of managed pressure drilling and considering fluid conservation, we obtain the following equation:

$$M\mathrm{d}q_{\mathrm{E}}=M_{\mathrm{G}}\mathrm{d}q_{\mathrm{GE}}+M_{\mathrm{L}}\mathrm{d}q_{\mathrm{LE}} \tag{2}$$

where, M is the mass flow of gas and drilling mud in the annular of MPD ($\mathrm{m^3/h}$); M_{L} is the liquid mass flow rate ($\mathrm{m^3/h}$) in the annulus of managed pressure drilling. M_{G} is the mass flow rate of gas phase in the annulus of managed pressure drilling ($\mathrm{m^3/h}$).

In this context, the transfer of heat from the two phases of gas and drilling mud to the surroundings can be expressed as follows

$$\mathrm{d}q_{\mathrm{E}}=\frac{K\pi D(T-T_0)}{M}\mathrm{d}H \tag{3}$$

In the formula, K is the total heat transfer coefficient of the fluid ($\mathrm{W/m^2\cdot K}$); D is the effective annular diameter of MPD (m); T is the fluid temperature (K); T_0 is formation temperature (K); H is the well depth (m).

Transfer heat from the gas to the surroundings can be expressed as follows

$$\mathrm{d}q_{\mathrm{GE}}=c_{\mathrm{PG}}\mathrm{d}T-c_{\mathrm{PG}}k_i\mathrm{d}p \tag{4}$$

where, k_i is the Joule-Thomson coefficient (°C/Pa); c_{PG} is gas heat capacities at constant pressure, (J/(kg·°C)); p is pressure (MPa).

Transfer heat from the drilling mud to the surroundings can be expressed as follows

$$\mathrm{d}q_{\mathrm{LE}}=c_{\mathrm{L}}\mathrm{d}T-\Gamma g\mathrm{d}H \tag{5}$$

Here, Γ is hydraulic gradient (m/m), which can be expressed as follows

$$\Gamma=(P_{\mathrm{R}}-P_{\mathrm{Z}})/(g\rho_{\mathrm{L}}H) \tag{6}$$

where, c_{L} is specific heat capacity for drilling mud (J/(kg·°C)); P_{z} is terminal pressure (MPa); P_{R} is starting point pressure (MPa); g is

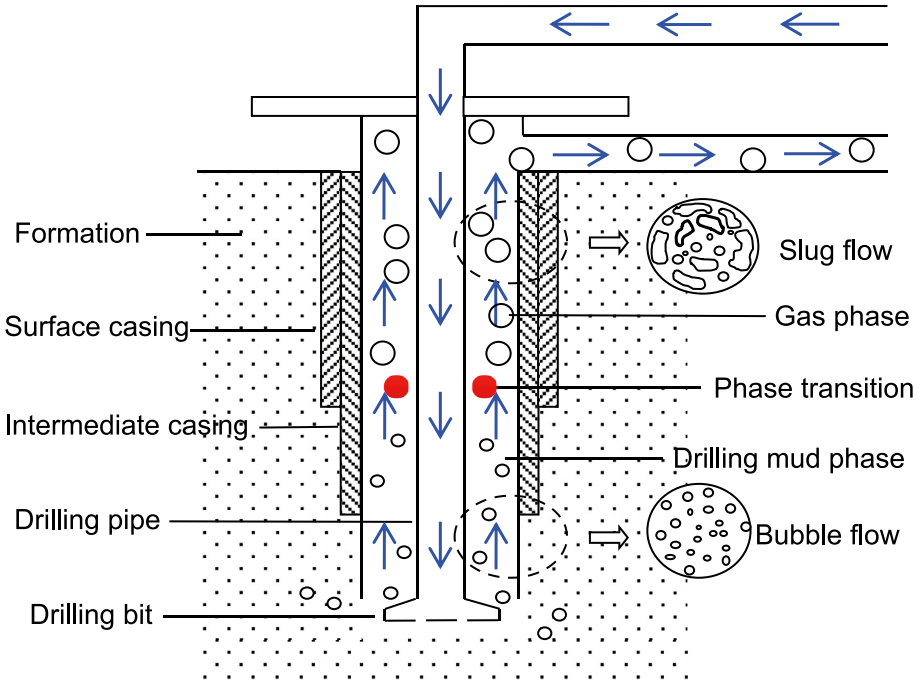

Fig. 1. Physical model of drilling fluid circulation when gas influx occurs.

the acceleration of gravity (m^2/s); ρ_L is drilling mud density (kg/m^3).

2.3. Physical equations

2.3.1. Critical parameters of the PT

Considering the phase transition (PT) of the supercritical fluid, it is essential to ensure that the critical pressure and critical temperature of the supercritical fluid are defined by the following relationship presented by Hasan and Kabir (2012).

$$p_{pc} = \sum_{i=1}^{n} y_i p_{ci} \tag{7}$$

where, p_{pc} is critical pressure (MPa); y_i is the mole fraction for components i; p_{ci} is the critical pressure at node i.

$$T_{pc} = \sum_{i=1}^{n} y_i T_{ci} \tag{8}$$

where, T_{ci} is the critical temperature of annulus node i of MPD; T_{pc} is the annular critical temperature of MPD (K).

Due to the presence of carbon dioxide, hydrogen sulfide gas, and a certain amount of non-hydrocarbon gases in the acid gas, computing critical parameters using conventional gas Kay's mix rules will result in a greater error. Wichert and Aziz proposed a correction method for acid gas containing CO_2 and H_2S. The correction method used to calculate the critical parameter for the acidic gas can be expressed as follows (Yarborough and Hall, 1974).

$$\begin{gathered} \varepsilon = \left[120\left(A^{0.9} - A^{1.6}\right) + 15\left(B^{0.5} - B^{4}\right)\right] \Big/ 1.8 \\ P_{pc}{}' = P_{pc}T_{pc}{}' \Big/ \left[T_{pc} + B(1-B)\varepsilon\right] \\ T_{pc}{}' = T_{pc} - \varepsilon \end{gathered} \tag{9}$$

where, P_{pc}' is corrected critical pressure (MPa); A is the mole fraction of hydrogen sulfide and carbon dioxide in the overflow gas; B is the mole fraction of hydrogen sulfide in the natural gas of overflow gas, T_{pc} is critical temperature (K); ε is correction factor.

2.3.2. Equations of state for drilling mud

By using the empirical formula of temperature and pressure, the density of drilling fluid at various temperatures can be determined.

If $T < 130$ °C, the density of drilling mud can be obtained by the following equation:

$$\rho_L = \rho_0\left(1 + 4\times10^{-10}P - 4\times10^{-5}T - 3\times10^{-6}T^2\right) \tag{10}$$

where, ρ_0 is fluid density at standard atmospheric pressure (kg/m^3).

If $T \geq 130$ °C, the density of drilling mud is:

$$\rho_L = \rho_0\left[1 + 4\times10^{-10}p - 4\times10^{-5}T - 3\times10^{-6}T^2 + 0.4\left(\frac{T-130}{T}\right)^2\right] \tag{11}$$

2.3.3. Equations of state for gas

Dranchuk and Abou-Kassem (1975) proposed the compression factor formula, and the compression factor under low pressure ($P < 35$ MPa) is expressed as.

$$\begin{aligned} Z_G = 1 &+ \left(0.3051 - \frac{1.0467}{T_r} - \frac{0.5783}{T_r^3}\right)\rho_r \\ &+ \left(0.5353 - \frac{02.6123}{T_r} - \frac{0.6816}{T_r^3}\right)\rho_r^2 \end{aligned} \tag{12}$$

where, $T_r = \frac{T}{T_c}$, $p_r = \frac{p}{p_c}$, $\rho_r = \frac{0.27p_r}{Z_G T_r}$.

By employing the compression factor formula proposed by Yarborough and Hall, the compression coefficient under high pressure (P>=35 MPa) can be expressed as follows:

$$Z_G = \frac{0.06125 P_r T_r^{-1} \exp\left[-1.2\left(1-T_r^{-1}\right)^2\right]}{Y} \tag{13}$$

where, Y is given by

$$\begin{aligned} &-0.06125 P_r T_r^{-1} \exp\left[-1.2\left(1-T_r^{-1}\right)^2\right] + \frac{Y+Y^2+Y^3+Y^4}{(1-Y)^3} \\ &= \left(14.76 T_r^{-1} - 9.76 T_r^{-2} + 4.58 T_r^{-3}\right) Y^2 \\ &- \left(90.7 T_r^{-1} - 242.2 T_r^{-2} + 42.4 T_r^{-3}\right) Y^{\left(2.18+2.82 T_r^{-1}\right)} \end{aligned} \tag{14}$$

The equation of state can be expressed as:

$$\rho_G = P / (Z_G \cdot R \cdot T) \tag{15}$$

In the formula, Z_G represents the gas compression factor; ρ_G represents the density (kg/m^3); R is the constant of EOS (J/kg·K); T is temperature (K).

2.4. Flow pattern analysis

The annular fluid flow characteristics are influenced by managed pressure drilling. It is assumed that the annular flow can be divided into bubble flow or slug flow. According to the Orkiszewski criterion (Orkiszewski, 1967).

For bubbly flow,

$$\frac{q_G}{q_M} < L_B \tag{16}$$

For slug flow,

$$\frac{Q_G}{Q_M} > L_B, N_{GV} < L_S \tag{17}$$

In the formula, Q_G is the gas volume flow rate (m^3/s); Q_M is the volume flow of drilling mud (m^3/s). L_B and L_S are both composed of dimensionless numbers

$$L_B = 1.071 - \frac{0.7277 v_m^2}{D} \tag{18}$$

where, v_m represents the fluid flow rate (m/s).

$$L_S = 50 + 36 N_{GV} Q_L / Q_G \tag{19}$$

where, Q_L represents the liquid volume flow rate (m^3/s).

The N_{GV} can be expressed as

$$N_{GV} = v_S \left(\frac{\rho_L}{g\sigma_S}\right)^{0.25} \tag{20}$$

In the model, g represents the acceleration of gravity (m^2/s); σ_S is the gas-liquid surface tension (N/m^2).

The average density of the two-phase flow can be expressed as:

$$\rho_m = \varphi_L \rho_L + \varphi_G \rho_G \tag{21}$$

In the model, ρ_m is the average density (kg/m^3). φ_G is the gas holdup in the gas phase; φ_L is the liquid gas holdup.

The annular air contains a fraction of liquid:

$$\varphi_L = 1 - \varphi_G \tag{22}$$

2.4.1. Bubble flow

The gas holdup of bubble flow can be expressed as:

$$\varphi_G = \frac{v_{SG}}{S_G(v_{SG} + v_{SL}) + v_{Gr}} \tag{23}$$

In the model, v_{SG} is the apparent velocity of gas (m/s); v_{SL} is the apparent velocity of the liquid phase (m/s).

The S_G value in bubble flow can be expressed as

$$S_G = 1.20 + 0.371\left(\frac{D_i}{D_o}\right) \tag{24}$$

where, D_i is the annulus inner diameter (m); D_o is denoted by annulus outer diameter (m).

The v_{Gr} velocity of the gas in the bubble flow can be expressed as

$$v_{Gr} = 1.53\left[\frac{g\sigma_S(\rho_L - \rho_G)}{\rho_L^2}\right]^{0.25} \tag{25}$$

2.4.2. Slug flow

The S_G of the gas in the slug flow can be expressed as

$$S_G = 1.182 + 0.9\left(\frac{D_i}{D_o}\right) \tag{26}$$

The v_{Gr} velocity of the gas in the slug flow can be expressed as

$$v_{Gr} = \left(0.35 + 0.1\frac{D_i}{D_o}\right)\left[\frac{gD_o(\rho_L - \rho_G)}{\rho_L}\right]^{0.5} \tag{27}$$

3. The temperature model developed

It can be obtained according to Eq. (1):

$$\frac{dp}{dz} = \rho_m g \sin\theta - \frac{\tau_w \pi D}{R} - \rho_m v_m \frac{dv_m}{dz} \tag{28}$$

where, θ is tilt angle (°); τ_w is frictional pressure coefficient; R is annulus effective cross area (m^2); z is variable of distance from surface (m).

The deformation of the above formula can be obtained:

$$\rho_m v_m \frac{dv_m}{dz} = -\frac{\rho_m v_m v_{SG}}{p}\frac{dp}{dz} = -\frac{W_m q_G}{A^2 p}\frac{dp}{dz} \tag{29}$$

where, W_m is mass flow velocity (kg/m^3); A is annulus effective cross area (m^2); p is pressure (MPa).

The deformation of the above formula can be obtained:

$$\frac{dp}{dz} = \frac{\rho_m g + \tau_f}{1 - W_m Q_G / \left(A^2 p\right)} \tag{30}$$

where, τ_f is frictional pressure gradient (Pa/m).

Equations (2)–(6) may be simplified into Eq. (31).

$$k\pi D(T-T_0)\mathrm{d}H = M_G c_{pG}\mathrm{d}T - M_G c_{pG} D_i \mathrm{d}p + M_L(c_L \mathrm{d}T - \Gamma g \mathrm{d}H) \tag{31}$$

Pressure loss of the system in length element dH is

$$\mathrm{d}p = \frac{P_R - P_Z}{H}\mathrm{d}H \tag{32}$$

Equation (3) may be simplified as follows

$$\mathrm{d}T = a(T - T_0 - b)\mathrm{d}H - J\frac{xc_{pG}}{c_p}\left(\frac{P_R - P_Z}{H}\right)\mathrm{d}H \tag{33}$$

Here, $c_p = xc_{pG} + (1-x)c_{pL}$, $b = \frac{(P_R - P_Z)(1-x_{wg})}{ac_p\rho_L H}$, $a = \frac{K\pi D}{Mc_p}$.

With x_{wg} is the quality of void fraction; J is the Joule-Thomson coefficient.

4. Solution of the temperature model

The temperature solution procedure for MPD operations is depicted in Fig. 2. The boundary conditions for the multiphase flow solution were derived by monitoring the wellhead overflow, outlet density, and physical properties of the fluid:

$$\begin{aligned} &\frac{\mathrm{d}p}{\mathrm{d}z} = F(z,p) \\ &p(z_0) = P_0 \end{aligned} \tag{34}$$

With the initial value (z_0, P_0) and the function $F(z, p)$, Eqs. (35)–(38) can be obtained.

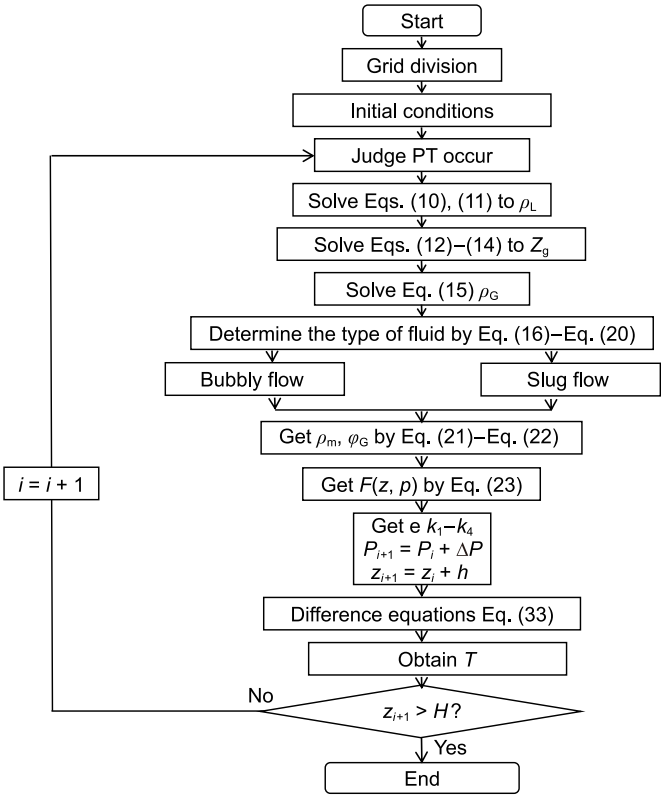

Fig. 2. Solution procedure for temperature in MPD operations.

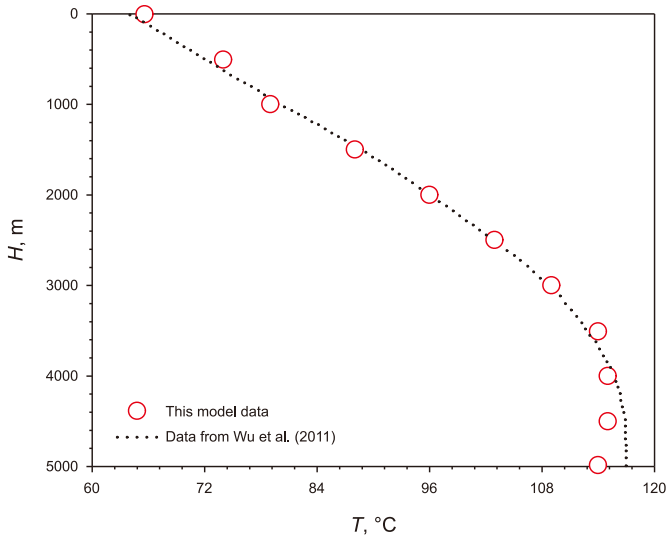

Fig. 3. The predicted temperature was verified with the literature (Wu et al., 2011).

$$k_1 = F(z_0, p_0) \tag{35}$$

$$k_2 = F\left(z_0 + \frac{h}{2}, p_0 + \frac{h}{2}k_1\right) \tag{36}$$

$$k_3 = F\left(z_0 + \frac{h}{2}, p_0 + \frac{h}{2}k_2\right) \tag{37}$$

$$k_4 = F(z_0 + h, p_0 + hk_3) \tag{38}$$

where, h is the step of well depth. The pressure on the nod i+1 can be obtained by

$$p_{i+1} = p_i + \Delta p = p_i + \frac{h}{6}(k_1 + 2k_2 + 2k_3 + k_4) \tag{39}$$

$$T_R = (T_0 + b) + (T_z - T_0 - b)\mathrm{e}^{aL} - D_i\frac{x_{wg}c_{pg}}{c_p}\left(\frac{P_R - P_Z}{aL}\right)\left(1 - \mathrm{e}^{aH}\right) \tag{40}$$

With $a = \frac{k\pi D}{Mc_p}$, $b = \frac{(P_R - P_Z)(1-x_{wg})}{ac_p\rho_L L}$, $c_p = x_{wg}c_{pg} + (1-x_{wg})c_{pl}$, $D_i = \frac{(0.98\times10^6/T_{pj}^2 - 1.5)}{10^9 c_{pg}}$.

The predicted temperature was validated against the literature (Wu et al., 2011), and the results showed consistency.

5. Analysis and discussion

Solving the multiphase flow model, inputting wellbore geometry and drilling tool combination parameters, and calculating relevant multiphase fluid parameters and formation properties, discrete spatial parameters are computed as per calculation requirements. Concurrently, the flow states of each phase during steady-state flow and the wellbore temperature are calculated as initial conditions for solving the phase transition points. The computational process involves solving control units at the inflow boundary, followed by upward calculation from the bottom to the top, and finally solving control units at the outflow boundary. After completing a time step, the data is stored as the initial conditions for the next time step, and this cycle continues until the calculated

time reaches the predetermined duration. Obtaining wellbore phase transition points involves the following main steps.

(1) Discretize the annulus into n grid cells, and for each discrete cell i, solve the multiphase flow model using a semi-explicit finite difference method;
(2) Obtain parameters such as annulus multiphase flow void fraction, gas-liquid density, gas slip velocity, etc.
(3) Substitute the fundamental multiphase flow parameters for each cell i into the temperature field mathematical formula to derive the temperature field for discrete cell i;
(4) Package the multiphase flow model computation module and the computation of the multiphase temperature field model;
(5) In accordance with the grid sequence, determine phase transitions by referencing fitting models for phase transition temperature and pressure;
(6) If the solution accuracy meets the requirements, the calculation concludes. If not, densify the wellbore grid (see Fig. 3 and Table 1).

Take an experimental well in Sichuan Province as an example. When the well was drilled to 4000 m, the well body structure and drilling assembly were shown in Fig. 4. The drilling fluid is pumped in from the riser and flows through the kelly, drill pipe, and drill collar to the bottom of the hole and back to the surface along the annulus. The flow rate of gas and liquid can be monitored in real time through coriolis flow rate, and the initial data of back pressure can be monitored in real time through pressure sensor. Taking a gas well in Xinjiang Uygur Autonomous Region of China as an example, the depth of the well is 4000 m. See Table 2 for gas-mud properties (density and viscosity), borehole structure, well design parameters

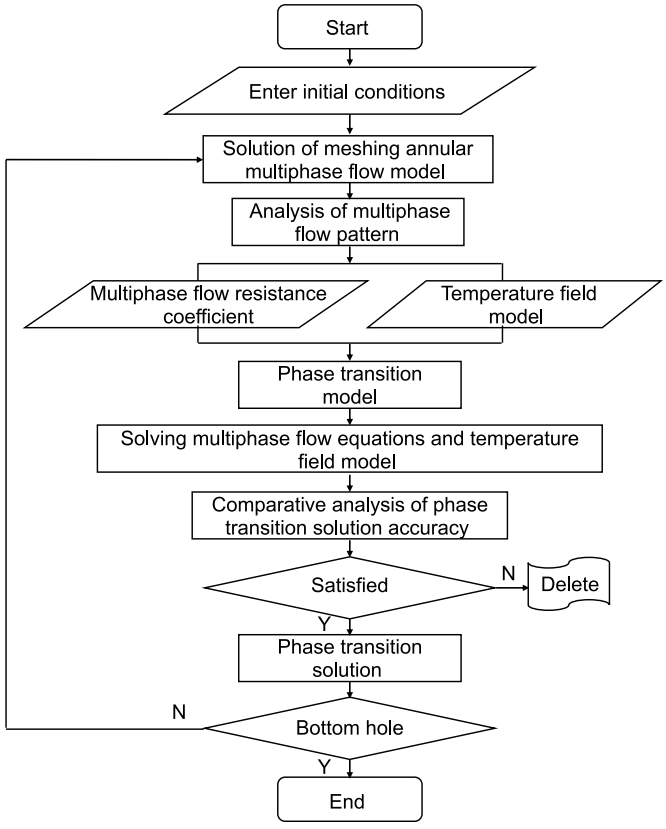

Fig. 4. Annulus multiphase phase transition point solving technique roadmap.

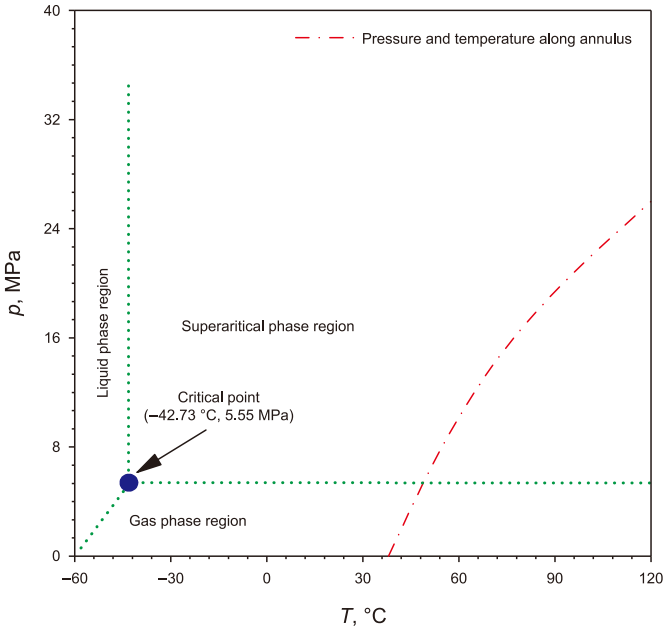

Fig. 5. The phase diagram variation with pressure and temperature.

(depth and diameter) and calculated well operation (see Fig. 5).

CO_2 exhibits a density abrupt change near its critical point, displaying nonlinearity, whereas methane density is approximately linear. The main reason is that methane has a very low critical temperature, making it unlikely for reservoir conditions to be near methane's critical temperature point. Methane has a large temperature contrast, resulting in its approximate behavior as an ideal gas within the entire exploration and development range of the reservoir. When CO_2 is in the gas state, its viscosity increases with rising temperature. Under high pressure, CO_2 viscosity differs from low pressure behavior, increasing with pressure and decreasing with temperature. The viscosity variation near the critical point is significant, and for CO_2 in a supercritical state, its viscosity is higher than that of gaseous CO_2.

5.1. Analysis of the PT point

Figs. 6 and 7 graphically interpret the pressure distributions along the flow direction in the annulus. The pressure first sharply decreases at the bottomhole and then slightly decreases along the flow direction near the wellhead. Gas phase transition occurs when the mixture of influx gas migrates to depths of 200–800 m. The flowing fluid undergoes a phase transformation from supercritical liquid to gas, leading to a rapid expansion of fluid volume in an extremely brief period. Figs. 6 and 7 display predictions for PT during gas influx in drilling operations, with a significant pressure change near PT. This is because, during the migration of influx gas from bottomhole to wellhead, the temperature and pressure gradually decrease. The pressure can reach about 56 MPa under high pressure in the bottomhole.

At a constant temperature, viscosity decreases as pressure reduces. At $T = 32$ °C, under the same pressure, CO_2 viscosity is higher than that of methane. Methane's viscosity behavior changes in an approximately linear manner, while CO_2 undergoes significant variations near its critical pressure. At the critical point of CO_2 ($T = 30.978$ °C, $P = 7.38$ MPa), its isothermal compressibility approaches infinity. When the system temperature is $T = 32$ °C and the pressure decreases from 10 to 7.5 MPa, the volume undergoes an unusually sharp change with pressure, resulting in a 3715%

Table 1
Physical and chemical properties of main components of acid natural gas.

Component	H_2S	CO_2	CH_4	C_2H_6	C_3H_8	n-C_4H_{10}	i-C_4H_{10}
Molar mass, kg/kmol	34.082	44.01	16.043	30.070	44.097	58.124	58.124
Critical temperature, K	373.55	304.128	190.564	305.5	370.00	425.39	408.11
Critical temperature, °C	100.4	30.978	−82.586	32.35	96.85	152.24	134.96
Critical pressure, MPa	9.008	7.3773	4.5992	4.8835	4.2568	3.7928	3.6480
The critical volume, m^3/kmol	0.0982	0.09412	0.09863	0.148	0.203	0.255	0.263
The critical density, kg/m^3	347.057	467.6	162.66	203.18	217.23	227.94	221
Critical deviation factor Z_C	0.284	0.274	0.288	0.283	0.285	0.274	0.283
Triple point temperature, K	186.65	216.35	90.7	89.9	85.5	134.8	113.6
Triple point temperature, °C	−86.5	−56.8	−182.5	−183.25	−187.65	−138.35	−159.55
The normal boiling point T_b, K	212.8	194.75	111.656	184.54	231.09	261.43	273.65
The normal boiling point T_b, °C	−60.4	−78.4	−161.494	−88.61	−42.06	−11.72	−0.5
Eccentric factor	0.1012	0.22394	0.01142	0.0986	0.1524	0.2010	0.1848

Table 2
Parameters of calculation well.

Type	Property	Value
The liquid phase	The liquid phase dynamic viscosity, Pa·s	0.056
	The liquid phase density, kg/m^3	1460
Gas	The gas relative density	0.65
	The gas viscosity, Pa·s	1.14×10^{-5}
Casing	Casing elastic modulus of string, Pa	2.07×10^{11}
	Casing poisson ratio of string	0.3
	Casing roughness, m	1.54×10^{-7}
The ground environment	The ground environment temperature, K	298
	Atmosphere pressure, MPa	0.101
Thermal conductivity	Formation, J/m·s·°C	1.717
	Drilling mud, J/m·s·°C	1.7307
Formation	Geothermal gradient, °C/m	0.020
Heat capacities at constant pressure	Gas, kJ/(kg·K)	1.005
	Drilling mud, kJ/(kg·K)	0.438

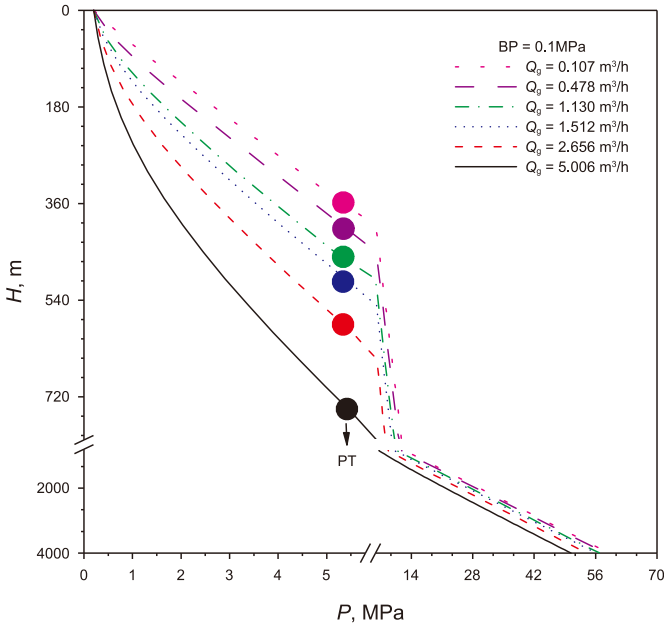

Fig. 6. Effect of gas influx rate on phase transition point.

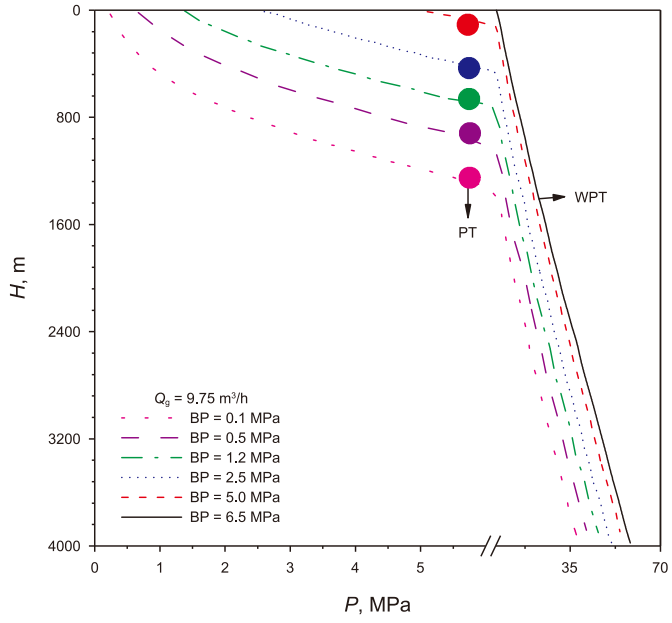

Fig. 7. Effect of BP on phase transition point.

increase in isothermal compressibility. In contrast, under the same conditions, methane's isothermal compressibility increases by only 33.5%. CO_2 exhibits roughly 120 times greater volumetric expansion capacity than methane due to fluid elasticity characteristics. These characteristics determine fluid compressibility and the extent of gas-liquid energy dissipation, thus affecting pressure, temperature, and phase transition points.

As a result, the gas exhibits low compressibility, leading to minimal changes in pressure due to gas volume fluctuations. This results in insignificant differences in pressure at positions far away from the wellhead. However, there is a significant change in void fraction in the bottomhole. PT occurs when the pressure in the

annulus is less than 5.55 MPa. Above the PT point along the annulus, a phase transition from liquid to gas occurs for the supercritical liquid phase. According to the EOS, as pressure decreases, the gas density decreases and the compressibility of gas increases. This leads to increased loss of interphase momentum and energy exchange, promoting interphase momentum exchange. Consequently, it contributes to the decrease of pressure along the annulus.

During the two-phase flow transport of gas and drilling fluid, the gas density is lower than that of the drilling fluid. The gas slip velocity gradually accelerates. For a given annulus depth, the void fraction increases compared to the previous moment. Due to the sensitivity of pressure wave speed to void fraction changes, as the gas column moves along the annulus from the wellbore bottom to the wellhead, the gas column lengthens. It gradually satisfies the phase transition pressure-temperature conditions. Through computational analysis, it is determined that reaching the phase transition point is more likely near 600 m at the wellhead.

5.2. Effect of BP on temperature

Fig. 8 presents the variations in annulus void fraction under different backpressures (0.1–6.5 MPa). Fig. 9 illustrates the effects of different backpressures (0.1–6.5 MPa) on the annulus temperature field. The critical temperature increases with the growing number of carbon atoms, while the critical pressure decreases. For fluids existing in a supercritical state, once the external temperature and pressure reach the critical temperature and critical pressure, a phase transition occurs, transforming the supercritical fluid into a conventional gaseous state. The critical temperature and pressure for each component are calculated using the quasi-critical parameters and Kay's mixing rules.

When the back pressure value increases, and the temperature of two-phase flow decreases. The increased BP value is equivalent to the BP value of the entire annular closed space drilling fluid circulation system. Pressure moves from the wellhead to the bottom of the hole, so pressure increases in the annulus. According to the equation of state, with the increase of annulus pressure, gas density increases and gas compressibility decreases. Therefore, the loss of

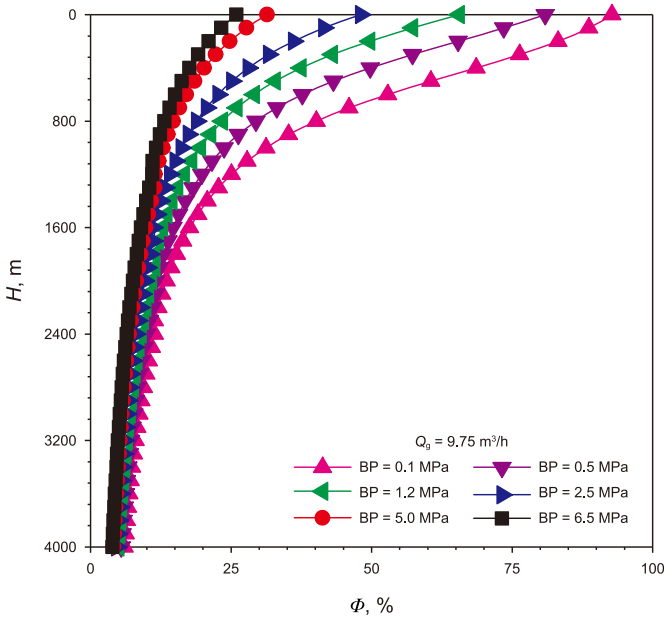

Fig. 8. Variation in annulus void fraction.

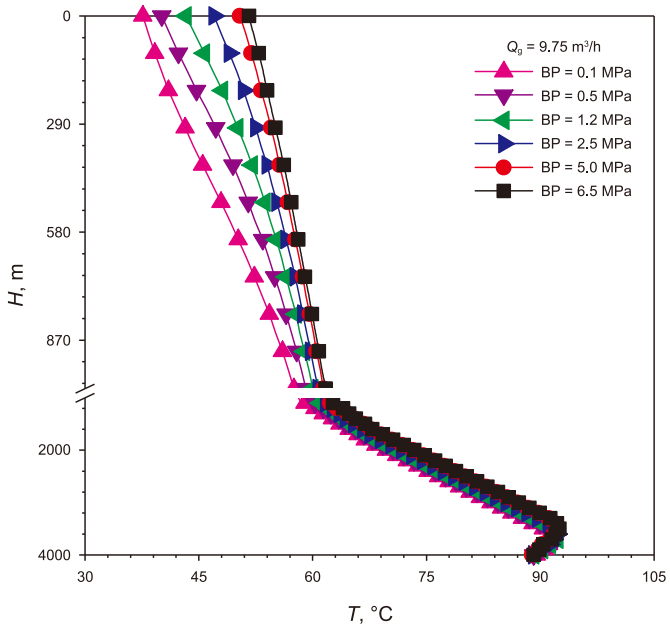

Fig. 9. Variation in annulus temperature field under with different backpressures. different backpressures.

interphase momentum and energy exchange is reduced, and the thermal conductivity is increased. It helps to increase temperature as pressure increases. In addition, due to the low compressibility of two-phase flow media under high pressure, the rising trend of temperature and the declining trend of gap ratio are slowed down in the range of high pressure controlled drilling back pressure.

As the invading fluid moves within the wellbore, the internal temperature and pressure gradually decrease. When the fluid reaches a depth of 550 m below its critical pressure, it undergoes a transition from a supercritical state to a gaseous state. Due to the critical temperature and pressure necessary for a rapid change being far from the occurring conditions, the fluid's properties do not exhibit significant alterations. Furthermore, there is no occurrence of an abrupt and dramatic volume expansion phenomenon. The degree of volume expansion of the actual fluid within the wellbore remains in close alignment with these conditions.

As a result, the loss of interphase momentum and energy exchange is reduced, while thermal conductivity is increased. This contributes to a temperature increase with pressure. Additionally, due to the low compressibility of two-phase flow media under high pressure, the rising trend of temperature and the declining trend of gap ratio are attenuated in the range of high-pressure controlled drilling back pressure. With the increasing well depth, the multiplication factor of wellbore gas volume shows a trend of initial growth followed by a decrease. This phenomenon is attributed to the gas being in a supercritical state under high-temperature and high-pressure conditions. After reaching a certain well depth, the gas volume experiences a sudden expansion.

5.3. Effect of gas influx rate on temperature

Fig. 10 demonstrates that gas content decreases with increasing well depth and increases with increasing bottom hole gas invasion. Fig. 11 reveals that the temperature initially increases with increasing well depth, then decreases, increases again, and finally decreases. Additionally, with increasing gas influx, the temperature of the entire annulus decreases.

With the increasing influx of gas at the wellbore bottom

(0.107–5.006 m^3/h), the annulus void fraction exhibits a trend of enlargement. At a depth of 600 m in the annulus, the gas volume undergoes rapid expansion. According to the PVT equation, as pressure and temperature decrease, the volume increases. Additionally, due to the phase transition of supercritical gas, it changes from a supercritical state to a gas state, resulting in a sharp volume expansion. Consequently, Fig. 11 depicts a significant increase in volume and annulus void fraction around a well depth of 600 m. As the gas influx rate increases, the temperature field demonstrates an overall decrease. When comparing the gas influx rates of $Q = 0.107$ and 5.006 m^3/h, the temperature at the wellhead rises from 44 to 59 °C, marking a temperature increase of 15 °C.

Table 3 presents a data list indicating changes in depth along with pressure and temperature. The calculated critical point of the mixed fluid (T_{pc}: −42.73 °C, P_{pc}: 7.55 MPa) is significantly distant from the wellbore temperature and pressure. Moreover, the critical temperatures of the mixed fluid are all beyond the range of wellbore temperatures, while the critical pressure of the mixed fluid is situated around a well depth of 550 m. Based on the calculation results, a phase transition occurs at 600 m, shifting from a supercritical state to a gaseous state. As per the gas state equation, with increasing pressure, the gas phase density gradually rises, enhancing the incompressibility of the gas-liquid two phases, thus increasing the wave speed. When pressure reaches high levels, gas compressibility changes minimally.

6. Results

This study involves the development of a set of numerical models to investigate the temperature of drilling mud in the annulus during circulation under gas influx conditions in drilling operations. The main conclusions are as follows.

(1) When the mixture of influx gas migrates to a depth of 200–800 m, gas phase transition occurs. The phase of the flowing fluid is transformed from supercritical liquid to gas, leading to rapid expansion of the fluid volume in an extremely brief period.

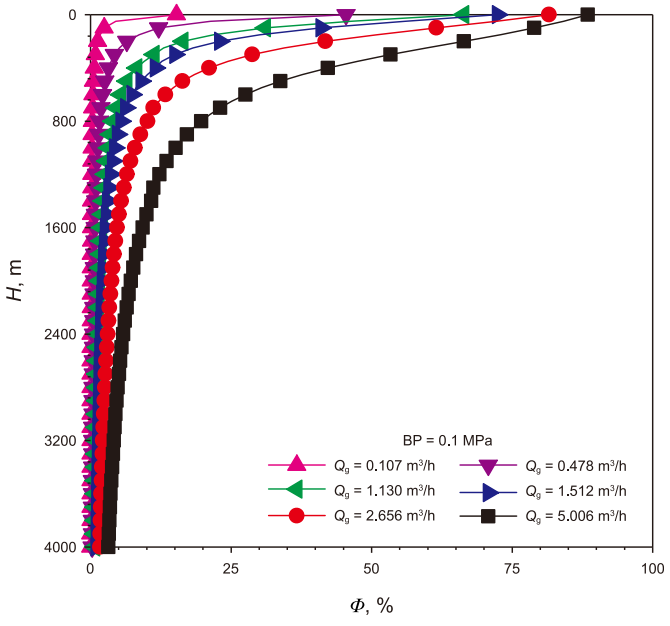

Fig. 10. Variation pattern along annulus void fraction.

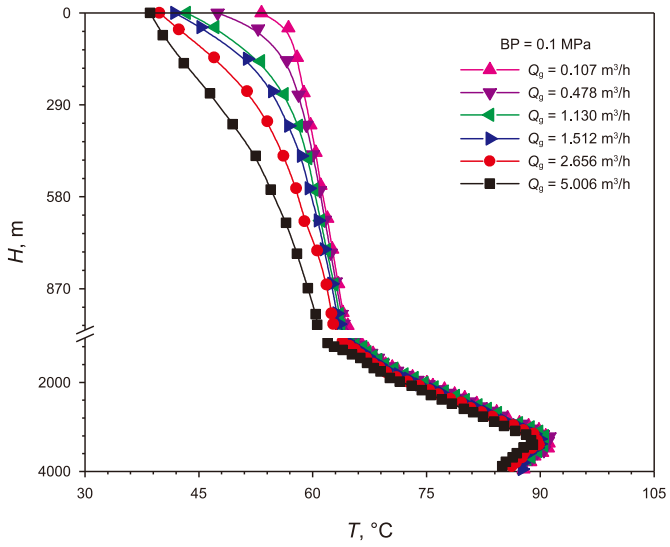

Fig. 11. Variation pattern along annulus temperature.

(2) According to the equation of state, an increase in annulus pressure results in higher gas density and reduced gas compressibility. Consequently, there is a decrease in the loss of interphase momentum and energy exchange, leading to enhanced thermal conductivity. This, in turn, contributes to temperature rise as pressure increases.

(3) With increasing well depth, the gas content decreases, and with increasing bottom hole gas invasion, the gas content increases. As the well depth increases, the temperature first increases, then decreases, increases again, and finally decreases. Additionally, with increasing gas influx, the temperature of the entire annulus decreases.

(4) As the invading gas fluid migrates, the temperature and pressure within the wellbore gradually decrease. When the fluid migrates to a depth below its critical pressure, approximately 550 m, it transitions from a supercritical state to a gaseous state. Due to the critical temperature and pressure necessary for a sharp transformation, the fluid properties do not significantly change, and there is no sudden volumetric expansion. This behavior closely corresponds to the actual volume expansion ratio of the fluid within the wellbore.

7. Discussions

(1) This paper only considers the changes in wellbore pressure caused by two flow types: bubble flow and slug flow. For the next step, annular flow and fog flow are recommended to be taken into account. The subdivision of flow types improves the accuracy of wellbore pressure calculation and leads to a more precise determination of wellbore temperature.

(2) This paper presents the mathematical model of the wellbore temperature field model. By incorporating empirical knowledge and computer programming, real-time wellsite prediction of wellbore temperature field changes is considered, along with the effects of supercritical fluid phase change. This allows for a more accurate understanding of changes in wellbore fluid phase behavior, greatly aiding in controlling overflow and ensuring the safety of drilling operations. The next step involves considering wellbore heat transfer and the influence of formation to further enhance

Table 3
Data list of depth, pressure, and temperature variations along the wellbore.

Well depth, m	Pressure, MPa	Temperature, °C	Phase transition	Well depth, m	Pressure, MPa	Temperature, °C	Phase transition
0	0	47.12	Gas state	1550	17.493	100.5492	Supercritical state
50	0.705	48.76	Gas state	1600	17.924	101.7467	Supercritical state
100	1.4	50.4	Gas state	1650	18.347	102.8659	Supercritical state
150	2.085	52.04	Gas state	1700	18.763	103.9033	Supercritical state
200	2.759	53.68	Gas state	1750	19.172	104.8554	Supercritical state
250	3.424	55.32	Gas state	1800	19.573	105.7186	Supercritical state
300	4.077	56.96	Gas state	1850	19.968	106.4893	Supercritical state
350	4.722	58.6	Gas state	1900	20.356	107.164	Supercritical state
400	5.356	60.24	Gas state	1950	20.737	107.7392	Supercritical state
450	5.981	61.88	Gas state	2000	21.111	108.2113	Supercritical state
500	6.597	63.63	Gas state	2050	21.478	108.5766	Supercritical state
550	7.203	65.6488	Gas state	2100	21.839	108.8318	Supercritical state
600	7.799	67.6641	Phase transition	2150	22.194	108.9731	Supercritical state
650	8.387	69.6722	Supercritical state	2200	22.541	108.9972	Supercritical state
700	8.965	71.6697	Supercritical state	2250	22.883	108.9003	Supercritical state
750	9.534	73.653	Supercritical state	2300	23.218	108.179	Supercritical state
800	10.094	75.6184	Supercritical state	2350	23.547	107.1296	Supercritical state
850	10.645	77.5626	Supercritical state	2400	23.87	104.7487	Supercritical state
900	11.188	79.4818	Supercritical state	2450	24.187	102.2327	Supercritical state
950	11.722	81.3726	Supercritical state	2500	24.497	98.878	Supercritical state
1000	12.248	83.2315	Supercritical state	2550	24.802	96.1811	Supercritical state
1050	12.765	85.0547	Supercritical state	2600	25.101	93.1384	Supercritical state
1100	13.274	86.8388	Supercritical state	2650	25.394	89.3464	Supercritical state
1150	13.775	88.5803	Supercritical state	2700	25.682	86.0014	Supercritical state
1200	14.267	90.2755	Supercritical state	2750	25.964	82.5	Supercritical state
1250	14.752	91.921	Supercritical state	2800	26.24	78.841	Supercritical state
1300	15.227	93.5131	Supercritical state	2850	26.51	75.0326	Supercritical state
1350	15.696	95.0484	Supercritical state	2900	26.776	71.0855	Supercritical state
1400	16.157	96.5231	Supercritical state	2950	27.036	67.0104	Supercritical state
1450	16.61	97.9339	Supercritical state	3000	27.29	63.818	Supercritical state
1500	17.055	99.2771	Supercritical state				

the accuracy of our wellbore temperature and phase change predictions.

Funding

The project support by the financial support of the National Nature Science Foundation of China (No.52274001, No. 52074018); China Petrochemical Corporation (No. p21069); The financial support of Fundamental Research Funds for the Central Universities (buctrc202017).

Conflicting interests

The authors declared no potential conflicts of interest with respect to the research, author-ship, and/or publication of this article. The authors have no conflicts of interest to declare that are relevant to the content of this article.

Ethics approval

This article does not contain any studies with animals performed by any of the authors. This article does not contain any studies with human participants or animals performed by any of the authors.

Data availability statement

The data that support the findings of this study are available from the corresponding author upon reasonable request.

CRediT authorship contribution statement

Yang Zhang: Data curation. **Yong-An Li:** Formal analysis. **Xiang-Wei Kong:** Formal analysis. **Hao Liu:** Software. **Teng-Fei Sun:** Writing – original draft, Methodology.

Subscripts

BP	Back pressure
EOS	Equations of state
HTHP	High temperature and high pressure
PT	Phase transition
MPD	Managed pressure drilling
WPT	Without phase transition
R–K4	The fourth order explicit Runge-Kutta

References

Agwu, O.E., Akpabio, J.U., Dosunmu, A., 2020. Artificial neural network model for predicting the density of oil-based muds in high-temperature, high-pressure wells. J. Pet. Explor. Prod. Technol. 10, 1081–1095. https://doi:10.1007/s13202-019-00802-6.

Ataga, E., Ogbonna, J., 2012. Accurate Estimation of Equivalent Circulating Density during High Pressure High Temperature (HPHT) Drilling Operations. In: SPE Nigeria Annual International Conference and Exhibition, Lagos, Nigeria. https://doi:10.2118/162972-MS.

Bacon, W.A., 2011. Consideration of compressibility effects for applied-back-pressure dynamic well control response to a gas kick in managed pressure drilling operations. MS Thesis. The University of Texas at Arlington.

Bennion, D.B., Bachu, S., 2006. Supercritical CO_2 and H_2S—Brine Drainage and Imbibition Relative Permeability Relationships for Intergranular Sandstone and Carbonate Formations. In: SPE Europe featured at EAGE Conference and Exhibition, Vienna, Austria. https://doi:10.2523/99326-MS.

Bennion, D.B., Bachu, S., 2008a. A Correlation of the Interfacial Tension between Supercritical Phase CO_2 and Equilibrium Brines as a Function of Salinity, Temperature and Pressure. In: SPE Annual Technical Conference and Exhibition, Denver, Colorado, USA. https://doi.org/10.2118/114479-MS.

Bennion, D.B., Bachu, S., 2008b. Drainage and imbibition relative permeability

relationships for supercritical CO_2/brine and H_2S/brine systems in intergranular sandstone, carbonate, shale, and anhydrite rocks. SPE Reservoir Eval. Eng. 11 (3), 487–496. https://doi:10.2118/99326-pa.
Bu, Y.H., Li, F., Wang, Z.Z., et al., 2011. Preliminary study on air injection in annuli to manage pressure during cementing. Procedia Eng. 18, 329–334. https://doi.org/10.1016/j.proeng.2011.11.052.
Choe, J., Juvkam-Wold, H.C., 1997. A modified two-phase well-control model and its computer applications as a training and educational tool. SPE Comput. Appl. 9 (1), 14–20. https://doi.org/10.2118/37688-PA.
Dranchuk, P.M., Abou-Kassem, H., 1975. Calculation of Z factors for natural gases using equations of state. Journal of Canadian Petroleum Technology 14 (3). PETSOC-75-03-03. https://doi:10.2118/75-03-03.
Fu, J., Su, Y., Jiang, W., et al., 2020. Multiphase flow behavior in deep water drilling: the influence of gas hydrate. Energy Sci. Eng. 8 (4), 1386–1403. https://doi.org/10.1002/ese3.600.
Hajidavalloo, E., Daneh-Dezfuli, A., Falavand Jozaei, A., 2021. Effect of temperature variation on the accurate prediction of bottom-hole pressure in well drilling. Energy Sources, Part A Recovery, Util. Environ. Eff. 1–21. https://doi.org/10.1080/15567036.2020.1797943.
Hasan, A.R., Kabir, C.S., 2012. Wellbore heat-transfer modeling and applications. J. Petrol. Sci. Eng. 86, 127–136. https://doi.org/10.1016/j.petrol.2012.03.021.
Kabir, C.S., Hasan, A.R., 1991. Heat Transfer during Two-phase Flow in Wellbore, Part I Formation Temperature. In: SPE Annual Technical Conference and Exhibition, Dallas, Texas. https://doi:10.2118/22866-MS.
Kumar, A., Samuel, R., 2012. Analytical Model to Estimate the Downhole Temperatures for Casing while Drilling Operations. In: SPE Annual Technical Conference and Exhibition. San Antonio, Texas, USA. https://doi:10.2118/159278-MS.
Li, J., Sun, J., Lv, K., et al., 2022. Nano-modified polymer gels as temperature-and salt-resistant fluid-loss additive for water-based drilling fluids. Gels 8 (9), 547. https://doi.org/10.3390/gels8090547.
Lin, Y., Kong, X., Qiu, Y., et al., 2013. Calculation analysis of pressure wave velocity in gas and drilling mud two-phase fluid in annulus during drilling operations. Math. Probl Eng., 318912. https://doi.org/10.1155/2013/318912.
Lordejani, S.N., Abbasi, M.H., Velmurugan, N., et al., 2020. Modeling and numerical implementation of managed-pressure-drilling systems for the assessment of pressure-control systems. SPE Drill. Complet. 35 (4), 598–619. https://doi.org/10.2118/201108-PA.
Orkiszewski, J., 1967. Predicting two-phase pressure drops in vertical pipe. J. Petrol. Technol. 19 (6), 829–838. https://doi.org/10.2118/1546-PA.
Pepin, G., Gonzalez, M., Bloys, J.B., et al., 2004. Effect of Drilling Fluid Temperature on Fracture Gradient: Field Measurements and Model Predictions. In: ARMA North America Rock Mechanics Symposium, Houston, Texas. ARMA.
Pu, L., Xu, P., Xu, M., et al., 2022. Lost circulation materials for deep and ultra-deep wells: a review. J. Petrol. Sci. Eng. 214, 110404. https://doi.org/10.1016/j.petrol.2022.110404.
Ramey Jr., H.J., 1962. Wellbore heat transmission. J. Petrol. Technol. 14 (4), 427–435. https://doi.org/10.2118/96-PA.
Saeed, S., Lovorn, R., Knudsen, K.A., 2012. Automated Drilling Systems for MPD—the Reality. In: IADC/SPE Drilling Conference and Exhibition. San Diego, California, USA. https://doi:10.2118/151416-ms.
Shiu, K.C., Beggs, H.D., 1980. Predicting temperatures in flowing oil wells. J. Energy Resour. Technol. 102 (1), 2–11. https://doi:10.1115/1.3227845.
Sleiti, A.K., Takalkar, G., El-Naas, M.H., et al., 2020. Early gas kick detection in vertical wells via transient multiphase flow modelling: a review. J. Nat. Gas Sci. Eng. 80, 103391. https://doi.org/10.1016/j.jngse.2020.103391.
Tarvin, J.A., Walton, I., Wand, P., et al., 1991. Analysis of a Gas Kick Taken in a Deep Well Drilled with Oil-Based Mud. In: SPE Annual Technical Conference and Exhibition, Dallas, Texas. https://doi.org/10.2118/22560-MS.
Thiessen, J.J., 2017. Drilling Mud Cooling System. USA Patent, 9617811B2.
Thompson, M., Burgess, T.M., 1985. The Prediction of Interpretation of Downhole Mud Temperature while Drilling. In: SPE Annual Technical Conference and Exhibition, Las Vegas, Nevada. https://doi.org/10.2118/14180-MS.
Vieira, P., Torres, F., Qamar, R.A., et al., 2012. Downhole Pressure Uncertainties Related to Deep Wells Drilling are Safely and Precisely Ascertained Using Automated MPD Technology. In: North Africa Technical Conference and Exhibition. Cairo, Egypt. https://doi.org/10.2118/150944-MS.
Wei, N., Pei, J., Xue, J., et al., 2022. Modeling of multiphase flow during underbalanced drilling considering velocity, temperature and pressure. Energy Rep. 8, 2574–2587. https://doi.org/10.1016/j.egyr.2022.01.160.
Wu, X.D., Wu, H., Han, G.Q., et al., 2011. A new model for calculating wellbore temperature and pressure distribution of a high-H_2S gas well considering the influence of the sulfur release in wellbores. Nat. Gas. Ind. 31 (9), 69–72. https://doi:10.3787/j.issn.1000-0976.2011.09.012.
Yarborough, L., Hall, K.R., 1974. How to solve equation of state for Z-factors. Oil Gas J. 72 (7), 86–88.
Yasunami, T., 2008. Numerical Temperature Prediction System in Injection Tubing, Bottom Hole and Reservoir Condition for Supercritical CO_2 Injection into Deep Coal Seams. In: SPE Annual Technical Conference and Exhibition, Denver, Colorado, USA. https://doi.org/10.2118/120201-STU.
Yin, Q., Yang, J., Li, Z., et al., 2020. A field case study of managed pressure drilling in offshore ultra high-pressure high-temperature exploration well in the South China Sea. SPE Drill. Complet. 35 (4), 503–524. https://doi.org/10.2118/191060-PA.
Zhang, Z., Xiong, Y., Pu, H., et al., 2021. Effect of the variations of thermophysical properties of drilling fluids with temperature on wellbore temperature calculation during drilling. Energy 214, 119055. https://doi.org/10.1016/j.energy.2020.119055.